Synthesis, Structural Features, and Reactivity of Fe−Mn Mixed Oxides Prepared by Microemulsion

T. Herranz,[†] S. Rojas,[†] M. Ojeda,[†] F. J. Pérez-Alonso,[†] P. Terreros,[†] K. Pirota,[‡] and J. L. G. Fierro*,[†]

Instituto de Catálisis y Petroleoquímica, CSIC C/Marie Curie, 28049 Cantoblanco, Madrid, Spain, and Departamento de Física Aplicada, Universidad Autónoma de Madrid (UAM), Cantoblanco, Spain

Received November 21, 2005. Revised Manuscript Received February 10, 2006

Iron−manganese mixed oxides have been prepared by the microemulsion (MEM) technique, obtaining solids displaying homogeneously distributed Fe−Mn phases. For the sake of comparison similar samples prepared by different techniques have been studied. Magnetization measurements reveal that the extension of the Fe−Mn interaction was enhanced in the samples prepared by microemulsion and so was the sample homogeneity. The average size of the oxide particles prepared by microemulsion lies in the nanometer range, displaying also a narrow particle size distribution. A certain degree of manganese surface enrichment was observed for all samples and overall in those containing a larger amount of Mn, irrespective of the preparation method as revealed by X-ray photoelectron spectroscopy. Selected solids were used as catalyst precursors for the Fischer−Tropsch reaction. Mn promotion led to an enhancement of the olefin-to-paraffin ratio in the samples over which Fe−Mn interaction developed.

1. Introduction

The preparation of Fe−Mn mixed oxides has attracted a great deal of attention as a result of their numerous applications such as superparamagnetic materials or as oxidation catalysts. Besides, Fe-based solids are already known as Fischer−Tropsch (FT) catalysts, producing gasoline, diesel, and waxes from a mixture of CO and H_2. Nowadays, because of the increasing price of crude oil, the FT process is attracting renewed attention.[1] Incorporation of manganese over Fe based catalyst reduces the formation of alkanes and favors the formation of low molecular weight hydrocarbons, and this was recognized as early as 1976.[2,3] In addition, an enhancement in the olefin selectivity has been reported for the manganese containing catalysts.[4] Nonetheless, the outcome of the promoting effect of the Mn depends on its concentration and its location within the catalyst.[5] It has also been reported that MnO acts as a structural promoter, increasing the stability of the catalyst.[6] However, most of these catalysts display a heterogeneous distribution of both iron and manganese oxide phases; whether such heterogeneity plays any role on the catalytic behavior of the samples has not been identified yet.

The preparation route of Fe−Mn mixed oxide precursors determines to a large extent their catalytic performance. It has been recognized that their activity depends on the synthesis procedure.[7,8] As a general rule, preparation of pure or mixed iron oxides catalysts as precursors for the FT reaction have been accomplished by coprecipitation of the iron nitrate precursors under a relatively well-controlled pH. Such a procedure usually renders a mixture of oxide phases randomly distributed, instead of the in principle more desirable solid oxide solution. Thus, exploring alternative preparation routes that would permit, at least to a certain degree, controlling the morphology of the samples, which permits a correlation between the catalytic performance and the morphology of such materials to be established, is still a challenge.

Microemulsion technology provides an attractive route to preparing mixed oxides displaying optimal textural properties, such homogeneous phase distribution, high specific area, and good stability.[9−11] The preparation of iron colloidal samples in inverse micelle solutions has been studied by Martino et al.[12] Also, the preparation of magnetite nanoparticles by the microemulsion technology has been recently reported.[13] Other authors have studied the preparation of magnetic materials such as spinel ferrites (MFe_2O_4 where M is a doping agent). Such materials are widely applied for

* Corresponding author. E-mail address: jlgfierro@icp.csic.es.
[†] CSIC.
[‡] Universidad Autónoma de Madrid.

(1) Dry, M. E. *Appl. Catal., A* **2004**, *276*, 1.
(2) Büssemeier, B.; Frohning, C. D.; Cornils, B. *Hydrocarbon Process.* **1976**, 105 and references therein.
(3) Maiti, G. C.; Malessa, R.; Baerns, M. *Appl. Catal.* **1983**, *5*, 151.
(4) Malessa, R.; Baerns, M. *Ind. Eng. Chem. Res.* **1988**, *27*, 279 and references therein.
(5) Maiti, G. C.; Malessa, R.; Löchner U.; Baerns, M. *Appl. Catal.* **1985**, *16*, 215.
(6) Hess, D.; Papp H.; Baerns, M. *Ber. Bunsen-Ges. Phys. Chem.* **1986**, *90*, 1234.
(7) Deckwer, W. D.; Serpemen, Y.; Ralek M.; Schmidt, B. *Ind. Eng. Chem. Process Des. Dev.* **1982**, *21*, 222.
(8) Suzdorf, A. R.; Kuznetsova, L. I.; Chumakov, V. G.; Chesnokov, N. V.; Kuznetsov, B. N. *React. Kinet. Catal. Lett.* **1984**, *26* (1−2), 183.
(9) Rojas, S.; Eriksson, S.; Boutonnet, M. In *Catalysis*; Spivey, J. J., Ed.; Specialist Periodical Series; Royal Society of Chemistry: London, 2004; Vol. 17.
(10) Eriksson, S.; Nylen, U.; Rojas, S.; Boutonnet, M. *Appl. Catal., A* **2004**, *265*, 207.
(11) Capek, I. *Adv. Colloid Interface Sci.* **2004**, *110*, 49.
(12) Martino, A.; Stoker, M.; Hicks, M.; Bartholomew, C. H.; Sault, A. G.; Kawola; J. S. *Appl. Catal., A* **1997**, *161*, 235.
(13) Lee, Y.; Lee, J.; Bae, Ch-J.; Park, J.-G.; Noh, H.-J.; Park, J.-H.; Hyeon, T. *Adv. Funct. Mater.* **2005**, *15*, 503.

10.1021/cm052568i CCC: $33.50
Published on Web 03/31/2006

Table 1. Sample Nomenclature[a]

catalyst	wt % H_2O	[Fe] (mol/L)	ω_0	oil phase	BET_{fresh} (m^2/g)	BET_{calcd} (m^2/g)	*d* (nm)	phase (calcined)
NP-70-1	5	0.1	5.5	isooctane	203			
NP-70-2	10	0.1	11.0	isooctane	117			
NP-70-3	10	0.5	11.0	isooctane	261	29		Fe_2O_3
NP-70-4	10	1.0	11.0	isooctane	287	37		Fe_2O_3
NP-70-5	10	0.7	11.0	isooctane		25	32.7	Fe_2O_3
NP-80-1	10	0.7	11.0	isooctane		47	37.3	Fe_2O_3
NP-90-1	10	0.7	11.0	isooctane		28	30.6	Fe_2O_3
TG-70-1	5	0.1	5.75	isooctane	213			
TG-70-2	10	0.1	11.5	isooctane	230			
TG-70-3	10	0.5	11.5	isooctane	301	45	am.	$MnFe_2O_4$
TG-70-4	10	1.0	11.5	isooctane	321	84	am.	$MnFe_2O_4$
TG-70-5	10	0.7	11.5	isooctane		56	am.	$MnFe_2O_4$
KB-70-3	10	0.7	n.d.	toluene		30	23.5	Fe_2O_3
DF-70-1	10	0.7	n.d	toluene		27	32.3	Fe_2O_3
X15-70-1	10	0.7	6.9	acetone		46	35.0	Fe_2O_3/Fe_3O_4 (traces)
AOT-70-1	10	0.7	12.3	isooctane		15	32.5/40.6[b]	Fe_2O_3/Mn_2O_3 (traces)
PM-1						25	24.4/17.4[c]	Fe_2O_3/MnO_2
CP-1						49	18.3/55.5[d]	Fe_2O_3
PM-2						1.8	181.0	Fe_2O_3

[a] For the microemulsion based samples the first two letters refer to the surfactant nature, the amount of Fe (atom %) comes next, and the suffix refers to the sample preparation number. Typical concentrations for the microemulsions are 20 wt % surfactant and 5−10 wt % water phase (containing the metal precursor). ω_0 is the water-to-surfactant molar ratio, PM stands for physical mixture, and CP stands for coprecipitation. Samples were calcined at 773 K; am. means amorphous solids. [b] Particle size for the bixbyite crystallites. [c] Particle size for the pyroluxite crystallites. [d] The particle size was measured after calcination a 973 K. Crystallite size was determined for one representative sample of each family applying the Debye−Scherrer equation to the $2\theta = 49.52°$ reflection. The last column summarizes the phases detected by the XRD analysis.

electronic applications. The preparation of $MnFe_2O_4$ nanoparticles from microemulsion has been reported by Liu et al.[14]

In this work, we have explored the preparation of Fe−Mn mixed oxides by means of the microemulsion technique and their application as FT catalysts. The influence of the surfactant, the water/surfactant molar ratio (ω_0), and the precursor concentration on the morphology of the samples were investigated. Materials were characterized by means of X-ray diffraction (XRD), X-ray photoelectron spectoscopy (XPS), Brunauer−Emmett−Teller (BET) analysis, Raman spectroscopy, thermogravimetric analysis (TGA)/differential thermal analysis (DTA), temperature-programmed reduction (TPR), and scanning and transmission electron microscopy (SEM and TEM) techniques. For the sake of comparison, reference materials prepared by coprecipitation or physical mixtures have been also prepared.

2. Experimental Section

2.1. Preparation of the Samples. $Fe(NO_3)_3 \cdot H_2O$, MnO_2, MnO, and $Mn(NO_3)_2$ were obtained from Aldrich and used as received. A series of surfactants with different HLB values were used. The HLB number is the hydrophilic-to-lipophilic balance number and accounts for the affinity of the surfactant either in water or in a nonpolar solvent. Tergitol 15-S-5 (labeled as TG) is a secondary alcohol ethoxylate (EO) with HLB = 10.5 (Dow Chemicals), Triton X-15 (labeled as X-15) is an octilphenol ethoxylate with HLB = 4.9 (Dow Chemicals), Tergitol NP4 (labeled as NP) is a nonylphenol ethoxylate with HLB = 8.9, Empilan KB2 (labeled as KB), a secondary alcohol ethoxylate with HLB = 8.1, and Triton TM DF12 (labeled as DF) with HLB = 10.6 have been used as nonionic surfactants. Sodium bis(2-ethylhexylsulfosuccinate) (AOT) has been utilized as the ionic surfactant. A series of Fe and Fe−Mn oxide based samples have been prepared by the microemulsion technique. The amount of Mn varied from 10 to 30 wt %. Analogous samples were prepared either by coprecipitation or by physical mixture of the oxide precursors. The amounts of $Fe(NO_3)_3$ and $Mn(NO_3)_2$ were set to obtain the desired concentration and Fe/Mn ratio. Although not necessary for the low precursor concentration microemulsions, a cosurfactant (ethanol) was added to increase the amount of the metal precursors stabilized within the polar phase of the microemulsion. Typically, the preparation of the microemulsion based samples was as follows: a water solution of the nitrate precursors $Fe(NO_3)_3$ and $Mn(NO_3)_2$ were added to a mixture of the oil and surfactant phase. After stirring, a transparent mixture, which indicates the formation of micelles of drop sizes between 2 and 20 nm,[15] stable at least for 24 h, was obtained. A water solution of NaOH was added as the precipitating agent. The mixture was left to decant overnight. The solid was recovered and washed thoroughly with distilled water and ethanol and dried overnight at 343 K. Samples were calcined at 773 K in air for 6 h. Such temperature was set according to the TGA results. The catalyst nomenclature and selected physical properties are summarized in Table 1. For the sake of comparison, similar reference samples were prepared by traditional routes. Solid labeled as PM-1 was prepared by mixing water solutions of $Fe(NO_3)_3$ and $Mn(NO_3)_2$ for 16 h and removing water in a rotary evaporator. Another reference sample, CP-1, was prepared by adding a NaOH (2 M) solution to a water solution of the metal precursors. Once the solid was obtained, it was washed thoroughly with water and ethanol and dried at 383 K. A further reference sample, labeled as PM-2, was prepared by physical mixture (milling in a mortar) of the oxide precursors. All samples were calcined at 773 K for 6 h. A pure hematite sample (labeled as 100Fe) was also prepared by precipitation of the nitrate precursor with NH_4OH under a controlled pH.

2.2. Characterization. The crystalline phases present in the samples and the crystal size have been determined by XRD. Powder samples were analyzed in an XRD apparatus equipped with a Guinier-Hägg camera with Cu $K\alpha_1$ radiation ($\lambda = 0.1542$ nm). The powder diffractograms of the various samples were recorded from 5 to 90° with a scanning rate 0.05°/s and acquisition time of 2 s. XPS spectra were acquired with a VG ESCALAB 200R spectrom-

(14) Liu, C.; Zou, B.; Rondinone, A. J.; Zhang, Z. J. *J. Phys. Chem. B* **2000**, *104* (6), 1141.

(15) Bourrel, M.; Schechter, R. S. *Microemulsions and Related Systems*; Marcel Dekker, Inc.: New York, 1988; Vol. 30.

eter in the pulse-count mode at a pass energy of 50 eV using a Mg Kα ($h\nu = 1253.6$) X-ray source. Kinetic energies of photoelectrons were measured using a hemispherical electron analyzer working in the constant pass energy mode. The background pressure in the analysis chamber was kept below 7×10^{-9} mbar during data acquisition. The powder samples were pressed into copper holders and then mounted on a support rod placed in the pretreatment chamber. The XPS data were signal averaged for at least 200 scans and were taken in increments of 0.1 eV with dwell times of 50 ms. Binding energies (BEs) were calibrated relative to the C 1s peak from carbon contamination of the samples at 284.6 eV to correct for contact potential differences between the sample and the spectrometer. High-resolution spectral envelopes were obtained by curve fitting synthetic peak components using the XPS peak software. The raw data were used with no preliminary smoothing. Symmetric Gaussian−Lorentzian product functions were used to approximate the line shapes of the fitting components.

TPR analyses of the fresh and calcined samples were performed in a Micromeritics TPD/TPR 2900 apparatus connected to a computer. In these experiments, 40 mg of the sample were introduced into the reactor and heated under He at 383 K for 1 h to remove physisorbed water. The TPR profiles were obtained in a 10% H_2/Ar flow (50 mL/min) from 298 to 1123 K at a rate of 10 K/min. H_2 consumption was measured with a thermal conductivity detector (TCD). The effluent gas was passed through a cold trap to remove water from the outlet stream.

TGA of the fresh samples was performed on a Mettler Toledo TGA/SDTA 851 apparatus. Typically, 30−40 mg of the sample was heated from 298 to 1373 K at a heating rate of 10 K/min under He or air atmosphere.

Specific area determination was carried out by analysis of the N_2 adsorption−desorption isotherms of the samples at the temperature of liquid N_2 with a Micromeretics ASAP 2000 apparatus. Samples were previously outgassed at 433 K for 24 h. Specific areas were calculated by applying the BET method to portions of the isotherms within the $0.05 < P/P_0 < 0.30$ relative pressure range.

SEM micrographs were obtained in a Philips XL30 equipped with an EDAX DX4i analyzer for energy-dispersive X-ray analysis at 20 keV to obtain quantitative information on the distribution of Fe and Mn atoms. Powdered samples were sputter coated with gold with a Sputter Coater SC502 previously to the analysis. Specimens for transmission electron microscopy (TEM) were ultrasonically dispersed in acetone. Analysis was conducted on a JEOL 2000 FX microscope.

Raman spectra were collected using a single monochromator Renishaw System 1000 equipped with a thermoelectrically cooled CCD detector and holographic super-Notch filter. A total of 20 mg of a powdered sample were mounted on a treatment chamber. The samples were excited with the 514.5 nm Ar line; the spectral resolution was about 3 cm^{-1}, and the spectrum acquisition time was 300 s.

Magnetization experiments were measured in a vibration sample magnetometer at room temperature.

Catalytic activity was measured in a reactor described elsewhere. Product analysis was performed on-line with a gas chromatograph (HP 5890) equipped with a TCD and flame ionization detector and two in-series capillary columns: SPB-5 (60 m × 0.53 mm) and Supel-Q Plot (30 m × 0.53 mm). This configuration allowed analyzing inorganic gases (H_2, CO, and CO_2), C_1-C_{16} hydrocarbons, C_1-C_{10} alcohols, and other oxygenated compounds.

3. Results and Discussion

At first, the study of the maximum amount of oxide precursor was accomplished. To this end, a series of microemulsions were prepared either with or without a cosurfactant, the latter being necessary for preparations containing a large amount of metallic precursor. The largest amount of solid precursor properly stabilized within a true microemulsion system was 0.7 M $Fe(NO_3)_3$. This amount is up to 50 times larger than that reported for similar preparations[12,14,16,17] and similar to the amount reported in ref 13 where authors claim such high amounts as a remarkable milestone for the preparation of a large amount of samples. Following this procedure the amount of sample that can be prepared from a single microemulsion was enhanced, thus reducing the potential harmful effect of the surfactant and oil phase by mass unit of prepared catalyst. Most of the aforementioned studies focused on the utilization of either ionic surfactants such as AOT, CTAB (cetyltrimethylammonium bromide), and so forth or surfactants of low HLB numbers. The present study has been conducted by employing nonionic surfactant, either NP or TG, and varying the ω_0 factor and the amount of cosurfactant.

$$\omega_0 = \frac{[\text{water}]}{[\text{surfactant}]} \tag{1}$$

Usually, by modifying the ω_0 factor particle size can be controlled because the size of the water droplet can be increased by water addition; nonetheless, the effect of the surfactant concentration should be taken into account as well.[18] As a general rule, when the water droplet size is increased more oxide precursor can enter into the water droplet, enhancing the amount of solid obtained from a single microemulsion. Within this scenario, the main issue would be to preserve the actual microemulsion phase itself, particularly, when a large amount of oxide precursor is employed the necessity of a cosurfactant is imperative.

For the samples prepared with either NP or TG as surfactants, the maximum amount of metal phase stabilized within a proper microemulsion are the samples labeled as NP-70-5 and TG-70-5, each sample containing a 0.7 M Fe concentration, the final stoichiometry of the solid being 70:30 (atom/atom) Fe/Mn. Microemulsions containing an Fe concentration larger than 1 M were not transparent mixtures despite large alcohol addition. No remarkable differences in the physicochemical properties of the samples as a function of the amount of metal in the microemulsion were found. Similar particle sizes were obtained as deduced by XRD analysis, and also the BET areas were similar for calcined samples. Essentially the same solids were obtained by microemulsion, irrespective of the amount of oxide precursor. Given the similar nature of the samples irrespective of the amount of metal precursor we will concentrate throughout this manuscript on the description and further study of samples NP-70-5 and TG-70-5. For the sake of simplicity, these samples will be referred to as NP-70 and TG-70, respectively.

(16) Fang, J.; Shama, N.; Tung, L.-D.; Shin, E.-Y, O'Connor, C. J.; Stokes, K. L.; Caruntu, G.; Wiley: J. B.; Spinu, L.; Tang, J. *J. Appl. Phys.* **2003**, *93* (10), 7483.
(17) Carpenter, E. E.; Sims, J. A.; Wienmann, J. A.; Zhou, W. L.; O'Connor, C. J. *J. Appl. Phys.* **2000**, *87* (9), 5615.
(18) Ojeda, M.; Rojas, S.; Boutonnet, M.; Pérez-Alonso, F. J.; García-García, F. J.; Fierro, J. L. G. *Appl. Catal., A* **2004**, *274*, 33.

However, a major difference was found between samples prepared from each series. As discussed below, the XRD patterns of samples prepared with NP reveal crystalline solids, while ill-formed crystalline solids were obtained when samples were prepared with TG as the surfactant. For the study of the influence of the surfactant, a series of samples have been prepared by varying the surfactant nature while for the rest the preparation parameters were identical to those of NP-70 and TG-70 preparations. Typically nonionic surfactants with HLB numbers between 6 and 10 were employed. For the nonionic surfactants, the HLB provides information with respect to emulsification of water and oil systems.[19] For the surfactant displaying a large HLB number, water-in-oil microemulsions were readily formed, except when a large amount of salt precursors (>0.7 M) were used over which ethanol has to be added to achieve a microemulsion. When Triton X-15 was used as the surfactant, a microemulsion was obtained only with acetone as the oil phase, probably as a result of the tendency of this surfactant for the oil phase. As expected, the nature of the surfactant regulates the microemulsion specifications and to some extent the particle size, but most importantly it played a strong influence on the nature of the samples. Results are discussed below.

Selected fresh and calcined samples were subjected to BET analyses; results are collected in Table 1. It could be observed that noncalcined samples displayed a large specific area where values as high as 300 m^2/g were found. In all cases, surface area decreased for calcined samples to values of 30−50 m^2/g. In general it can be said that microemulsion technology leads to Fe−Mn mixed oxides displaying larger BET surface area values than those samples prepared following more traditional routes.

TGA of the fresh samples was performed with the aim of obtaining information about the stability and phase transformation of the solids. For all samples a first weight loss occurred between 298 and 623 K; from this temperature and above samples were found to be stable. However, some samples (CP-1 and TG based ones) displayed some extra weight losses between 15 and 25 wt % at temperatures between 973 and 1123 K. The sample PM-2 displayed a weight gain at temperatures above 773 K, attributed to the presence of MnO phases, confirmed with the TGA profile of a commercial MnO sample. The DTA analysis of the samples displayed a strong exothermic peak centered between 453 and 553 K for the whole series. This behavior is characteristic of the transformation of ferrihydrite into hematite.[20] As shown in the next section, ferrihydrite was the only species detected in the diffractograms of the noncalcined samples in agreement with the thermal analysis. This would mean that, from precipitation, a ferrihydrite phase will be stabilized within the medium and further development to hematite or magnetite is retarded, but not impeded, by the presence of Mn^{2+} ions in solution.[21,22]

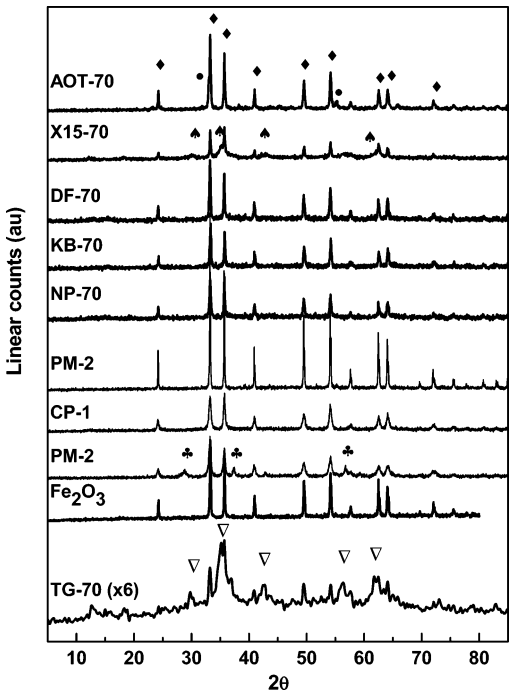

Figure 1. Diffractograms of selected samples calcined at 773 K under a nitrogen atmosphere. (◆) Fe_2O_3; (●) Mn_2O_3; (spades) Fe_3O_4; (clubs) MnO_2; (▽) $MnFe_2O_4$.

The XRD analysis of the noncalcined samples prepared by microemulsion displayed a diffractogram (not shown) characteristic of the two peaks of the ferrihydrite phase.[23] A ferrihydrite is an amorphous iron oxyhydroxide species whose actual composition is not accurately known.[24] However, as a result of the low degree of crystallinity of the samples and to the similar ionic radius of Fe^{3+} and Mn^{2+}, it was not possible to obtain further characterization details from the diffractograms. Two sets of diffractograms depicted in Figure 1 were obtained for the calcined (773 K in air) samples. On one hand, the catalysts prepared using Tergitol (TG) as the surfactant resulted in ill-formed crystalline solids, whose diffractograms reveal the coexistence of iron oxyhydroxide species, tentatively ascribed to a hydrohematite phase (JCPDS file 2-918). However, the presence of akaganeite (JCPDS file 8-93) and jacobsite [$(MnFe_2)O_4$] phases (JCPDS file 10-319) cannot be ruled out either. The lack of crystallinity of the solid, even after calcination, is in agreement with the role of Mn^{2+} ions, which are known to retard hematite formation,[21,22,25] suggesting that Fe−Mn ion interactions might be promoted over this preparation. Nonetheless, as a result of the lack of long-range order of the samples, an unequivocal conclusion cannot be established from the XRD analysis alone. At this calcination temperature, the development of relatively well-ordered phases would be expected instead of the presence of ferrihydrite type species. However, it has been recently proposed that, in Fe−Ce mixed oxides, the iron oxyhydroxide-like species can be stabilized,

(19) Griffin, W. C. *J. Soc. Cosmetic Chem.* **1949**, *1*, 311. (b) Griffin, W. C. *J. Soc. Cosmet. Chem.* **1954**, *5*, 259.
(20) Milburn, D. R.; Chary, K. V. R.; O'Brien, R. J.; Davis, B. H. *Appl. Catal., A* **1996**, *144*, 133.
(21) Cornell, R. M.; Giovaloni, R. *Clay Clay Miner.* **1987**, *39*, 11.
(22) Cornell, R. M.; Giovaloni, R. *Clay Clay Miner.* **1991**, *35*, 144.
(23) Zhao, J.; Feng, Z.; Huggins, F. E.; Shah, N.; Huffman, G. P.; Wender, I. *J. Catal.* **1994**, *148*, 194.
(24) (a) Janney, D. E.; Cowley, J. M.; Buseck, P. R. *Am. Mineral.* **2000**, *85*, 1180. (b) Janney, D. E.; Cowley, J. M.; Buseck, P. R. *Am. Mineral.* **2001**, *86*, 327.
(25) Tambor, J. L.; Dutrizac, J. E. *Chem. Rev.* **1998**, *98*, 2549.

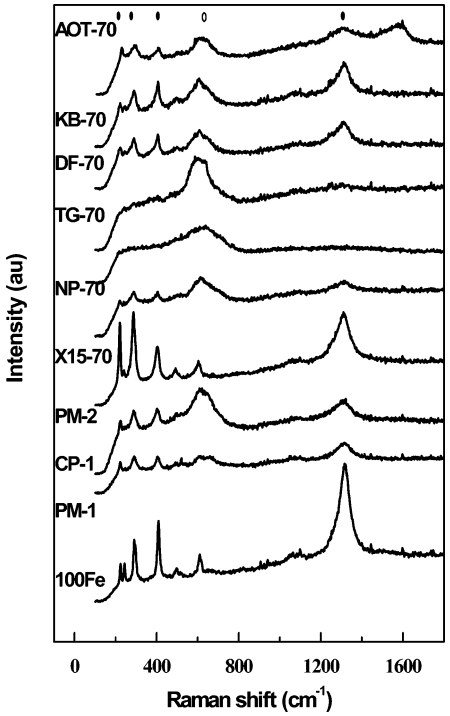

Figure 2. Raman spectra of selected samples (●) α-Fe_2O_3 and (○) γ-Fe_2O_3 and Fe_3O_4. Mn containing species are active within the same shift range.

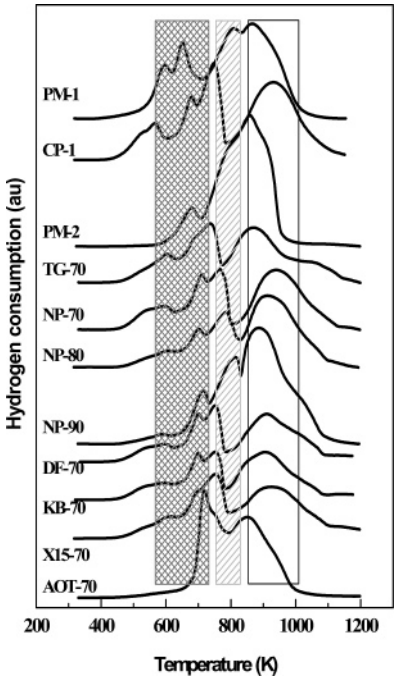

Figure 3. Hydrogen consumption profile of the calcined samples; reduction regions of the different species are highlighted as zones A, B, and C.

even after calcination, by interaction with foreign cations.[26] The role of Mn^{2+} might resemble the role of Ce cations as stabilizers of iron oxyhydroxide-like species.

On the other hand, the samples prepared with every other surfactant (NP, DF, KB, AOT, X-15) resulted in crystalline materials, whose diffractograms were consistent with the formation of hematite (α-Fe_2O_3). Neither Mn oxide nor Fe/Mn mixed oxide phases were detected by XRD analysis, except for samples AOT-70 (hematite and Mn_2O_3), X15-70 (jacobsite), and PM-1 (hematite and MnO_2). Nonetheless, even for these samples, the peaks of the diffractograms display broadening effects, reflecting a highly disordered cation arrangement of the samples calcined at lower temperatures;[27] after calcination at higher temperatures (973 K, XRD pattern not shown) this effect disappears yielding more crystalline solids.

Raman spectra, depicted in Figure 2, further confirm these results. Peaks from the α-Fe_2O_3 phases were detected in all cases, except in samples TG-70 and NP-70, as reflected by the set of bands centered between 200 and 500 cm^{-1}. A broad band centered at about 600−650 cm^{-1} accounts for the contribution of the Mn containing phases. This band is sharp in samples PM-2, 100Fe, and Mn_3O_4 (the latter not shown in the spectra) where no mixed Fe−Mn phases exist. Band broadening reflects contributions arising from single oxide phases, along with contributions due to the presence of amorphous Fe−Mn mixed oxide phases. The broadening of this band also accounts for the contribution of Mn species deposited on the surface of the solids[28] as much as from the presence of vacancies within the samples (as stated in the discussion of the XRD results). It has been reported that the Raman spectrum of the γ-Fe_2O_3 phase exhibits a band broadening effect when compared with the spectrum of α-Fe_2O_3, due to the vacancies of the former.[29] Some authors ascribe this broadening to MnO_2 species[28] while others claim MnO_2 to be a Raman inactive species.[30]

Sample NP-70 displays a broad band centered between 550 and 650 cm^{-1} pointing toward an enhancement of the Fe−Mn interactions in ill-formed crystalline phases; bands from any other iron or manganese phases were not detected. Nonetheless, bands from both hematite and Fe−Mn mixed oxides were detected for samples containing larger amounts of Fe than TG-70, that is in samples NP-80 and NP-90, suggesting that a decreasing amount of Mn ions facilitates iron oxide formation. This result is not confirmed by XRD analysis, suggesting the hematite nucleation is still impeded by the presence of Mn^{2+} cations, only to a lesser extent.

The hydrogen consumption profiles collected in Figure 3 show three groups of peaks centered at about 600, 700, and 900 K. The first set of peaks corresponds to the reduction of the Mn rich phases, jacobsite-type phases, as can be inferred by comparison of samples NP-70, NP-80, and NP-90; the greater the amount of Fe, the lesser the reduction peak. Despite containing amounts of Fe equal to those in the rest of the 70 series, samples PM-2 and AOT-70 showed no hydrogen consumption within this temperature range. As a matter of fact the TPR reduction profile of both samples is a combination of the reduction profiles of the Fe_2O_3 and

(26) Pérez-Alonso, F. J.; Granados, M. L.; Ojeda, M.; Terreros, P.; Rojas, S.; Herranz, T.; Fierro, J. L. G.; Gracia, M.; Gancedo, J. R. *Chem. Mater.* **2005**, *17*, 2329.
(27) Cornell, R. M.; Schwertmann, U. *The Iron Oxide*: *Structure, Properties, Reactions and Uses*; VCH Publishers: New York, 1996; Vol. 2, Chapter 14.
(28) Buciuman, F.; Patcas, F.; Cracium, R.; Zahn, D. R. T. *Phys. Chem. Chem. Phys.* **1999**, *1*, 185.
(29) Faria, D. L. A.; Silva, S. V.; Oliveira, M. T. *J. Raman Spectrosc.* **1997**, *28*, 873.
(30) Kapteijn, F.; Van Langeveld, A. D.; Moulijn, J. A.; Andreini, A.; Vuurman, M. A.; Turek, A. M.; Jehng, J. M.; Wachs, I. E. *J. Catal.* **1994**, *150*, 94.

Mn_3O_4 phases. The reduction process at about 700 K is ascribed to the transformation of Fe_2O_3 to Fe_3O_4 both in pure and in the Fe−Mn species highlighted as zones A and B, respectively, in Figure 3. Also, the Mn−spinel reduction would take place within this temperature range. Mn containing magnetite is further reduced to manganowustite at about 750 K, the temperature of the process depending upon the Fe−Mn interaction.[31] At about 800−900 K manganowustite ($Fe_xMn_{1-x}O$) phases are reduced to MnO and Fe^0, highlighted as zone C in Figure 3. At temperatures higher than 1100 K a shoulder, associated to the reduction of Fe^{2+} species located in the MnO lattice, appears. As a general rule, it was observed that the presence of Mn retarded the overall reduction process of Fe species.[32] The reduction profile of MnO_2 cannot be detected because it is overlapped by the rest of the processes except for the PM-1 showing reduction peaks at about 600 and 800 K. Despite the complex reduction profiles, it seems like Fe−Mn mixed oxide phases have been obtained, especially because the reduction of the hematite proceeded through a three steps process: first from hematite to magnetite (ca. 650 K), then to wustite at about 750 K, and at above 800 K to Fe^0. That is, wustite type species were stabilized. For instance, in the reduction profile of 100Fe (not shown) hematite reduction occurs in two steps, from hematite to magnetite (at ca. 650 K), and then in a single broad reduction step Fe^0 is obtained. Wustite is stabilized only when doping agents (Mn cations in this case) are incorporated in the FeO_x lattice.[32]

XPS analysis of the Fe 2p, Mn 2p, Na 1s (when present), C 1s, and O 1s core levels was evaluated from calcined samples subjected to different treatments: (i) nontreated and (ii) H_2/CO at 673 K. The analysis of selected used samples was also accomplished. An S-shaped background (Shirley) was used for evaluation of the Fe 2p and Mn 2p core levels.[33] In addition to the principal Fe $2p_{3/2}$ peak, a second component accounting for its asymmetry on the high BE side was also fitted and considered for the evaluation of the area of the Fe species. Charge effects were corrected by setting the C 1s peak at 284.6 eV and further confirmed by the position of the Na 1s peak at 1071.4 eV when possible. In this manner, the O 1s peak for metal oxide samples appeared centered at about 530.0 eV (not shown), as expected for transition metal oxides.[31−34] Other oxygen species centered at about 532.0 eV were also observed in the XPS spectra. Such species could be assigned either to molecular adsorbed oxygen or to hydroxyl or carbonyl groups.[31−34]

The only Fe species evident from the XPS analysis are assigned to oxidized Fe species, more likely Fe^{3+} type species (BE at ca. 711.0 eV). This assignment is supported by the shake up satellite component observed at ca. 719.2 eV, which is the fingerprint of the Fe^{3+} species. However, it cannot be firmly stated that other iron species are absent. Peak positions are collected in Table 2. The presence of oxidized iron species alone might be due to a surface oxidation process before the analysis as already reported.[31] Interestingly, in the Mn containing samples, the position of the Fe 2p core level peaks is slightly shifted toward higher BEs. The peak position for the O 1s core level was about 530.0 eV. In some samples an additional component at around 532.0 eV would point toward the existence of α-FeOOH species.[31] However, this hypothesis cannot be further confirmed from the XPS analysis alone, and results obtained from the thermal analysis clearly reveal that such species are not stable after calcination at 773 K. The analysis of the Mn 2p core level reveals the presence of a single peak centered at about 642.0 eV ascribed to Mn^{4+} species. After H_2/CO treatment at 673 K, the Mn 2p core level peak is shifted to about 640 eV and assigned to Mn^{2+} species.[35] The analysis of the Na 1s core levels reveal the presence of Na on the surface of the samples prepared using NaOH as the precipitating agent, namely, the microemulsion ones and CP-1. Na contamination is due to the precipitating agent, despite the thorough washing treatment. The amount of Na was comparable in all the samples,

Table 2. BE (eV) of Fe $2p_{3/2}$ and Mn $2p_{3/2}$, C 1s, and O 1s Core Electrons of Selected Samples[a]

sample	Fe $2p_{3/2}$	Mn $2p_{3/2}$	C 1s
100Fe	710.4		
PM-1	711.3	642.2	
PM-1(t)	710.7(73)	642.1	284.6(54)
	713.4(27)		285.7(25)
			288.3(22)
CP-1	710.8	642.3	
CP-1(t)	710.8	641.9	284.6(17)
			289.0(83)
CP-1(u)	707.1(41)	641.6	282.9(10)
	710.6(59)		284.6(70)
			286.0(20)
PM-2	710.6	traces	
PM-2(t)	710.5	traces	284.6(68)
			288.2(32)
NP-70	711.0	642.64	284.9(29)
			289.3(56)
			292.8(15)
TG-70	710.8	642.34	
TG-70(t)	710.9(66)	641.92	284.6(20)
	709.3(34)		290.7(80)
NP-90	711.1(78)	642.19	
	709.6(22)		
NP-90(t)	710.9(85)	642.20	284.6(15)
	709.5(15)		289.3(85)
DF-70	710.7	642.0	
DF-70(t)	709.8	640.4	284.6(29)
			285.9(18)
			289.1(53)
KB-70	710.7	642.0	
KB-70(t)	707.2(28)	640.3	283.1(24)
	709.5(72)		284.6(37)
			286.4(20)
			289.3(19)
AOT-70	710.9	642.0	
AOT-10(t)	707.2(9)	640.4	284.6(56)
	709.5(91)		286.1(26)
			288.7(18)
X15-70	711.0	642.1	
X15-70(t)	708.9	640.4	283.1(19)
			284.6(34)
			288.6(47)

[a] The C 1s value was set at 284.6 eV for charge corrections. When available, the Na 1s peak was used as the reference at 1071.4 eV. (t) Spectra obtained after treatment under H_2/CO at 673 K for 1 h. (u) Used sample.

(31) Wandelt, K. *Surf. Sci. Rep.* **1982**, *2*, 1.
(32) Leith, I. R.; Howden, M. G. *Appl. Catal.* **1988**, *37*, 75.
(33) Grosvenor, A. P.; Kobe, B. A.; Biesinger, M. C.; McIntyre, N. S. *Surf. Interface Anal.* **2004**, *36*, 1564.
(34) Linder, U.; Papp, H. *Appl. Surf. Sci.* **1988**, *32*, 75.
(35) Wagner, C. D.; Riggs, W. M.; Davis, L. E.; Moulder, J. F. *Handbook of X-ray Photoelectron Spectroscopy*; Perkin-Elmer Co.: Eden Prairie, MN, 1978.

Table 3. Atomic Ratios[a]

sample	Fe/Mn[b]	O/Fe[b]	O/Mn[b]	Fe/Mn[c] (atom %)
100Fe		4.17		
PM-1	0.64	6.25	4.00	0.20
PM-1				0.18
PM-1				0.86
PM-1				0.38
CP-1	0.58	5.26	2.96	0.63
CP-1				5.41
CP-1				2.17
CP-1				2.27
CP-1				2.79
PM-2		1.22		0.05
PM-2				7.46
PM-2				0.04
NP-70	0.55	7.14	4.00	2.34
KB-70	1.58			2.48
TG-70	0.65	5.00		2.34
DF-70	1.40			2.51
X15-70	1.38			2.22
AOT-70	0.79			2.23

[a−c] The Fe/Mn theoretical atomic ratio is 2.33. Atomic ratios were obtained from (b) XPS analyses and (c) EDX analysis. For the microemulsion based samples several analysis were used, but unlike for the CP and FM series, all displayed similar values.

and its effect on the activity of the catalyst precursors would be considered. The XPS analysis has been a very useful technique for the determination of the sample surface composition. The surface of the solid was enriched in Mn as evident from the analysis; results are depicted in Table 3. Similar results have been reported by other groups.[36]

When the samples are treated under a H_2/CO atmosphere at 673 K, similar spectra were obtained. Nonetheless, the amount of exposed Fe or Mn was lower, hardly detected in some cases, due to large carbon deposition on the surface of the samples as a result of the treatment. After the reduction treatment, the Fe/Mn atomic ratio increased with respect to the nontreated samples. This apparent contradiction reflects the effect of the nature of the reducing agent. While the previously reported experiments were conducted in H_2,[34] we have utilized a H_2/CO feed for the reduction treatment. A preferential carbonaceous deposition over Mn would explain the XPS results; however, such a phenomenon is unlikely because Fe is known to promote the formation of carbonaceous deposits. The position of the peaks is similar to that observed for the calcined samples.

Several samples were analyzed after reaction. Even if carbon removal was not complete it was possible to analyze Fe and Mn core levels. Fe was mainly in its oxidized state, most likely as Fe^{3+}, along with some Fe^{2+} pointing toward the coexistence of Fe_3O_4 and Fe_2O_3 species. Possibly the existence of Fe_2O_3 species might account for oxidation phenomena during the treatment of the samples. However, the most important finding was the presence of Fe^0 species that after analysis of the C 1s core level can be assigned as iron carbide species. The Mn $2p_{3/2}$ core level is centered at about 641 eV and ascribed to Mn^{2+} species. Fe $2p_{3/2}$ core level of sample CP-1 as representative of the series is depicted in Figure 4.

The results described so far point toward a rapid nucleation of ferrihydrite species [$FeO(OH)_x$] in the reaction medium

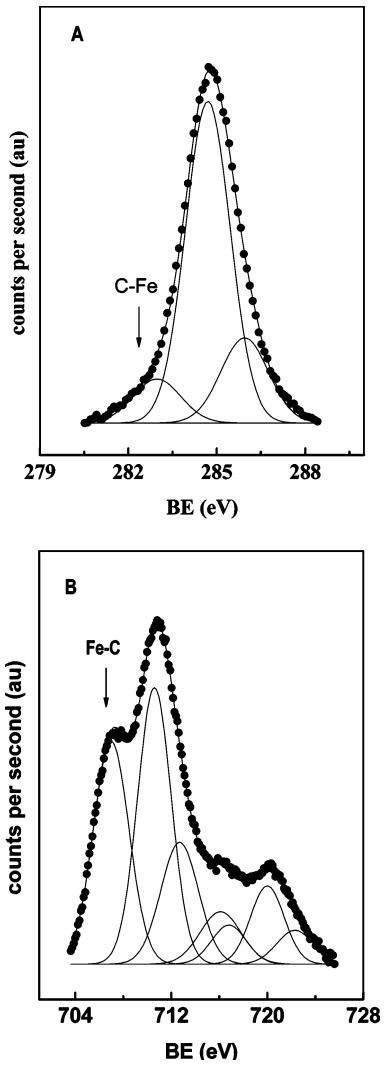

Figure 4. Graph corresponding to the C 1s (A) and Fe 2p (B) core level spectra of used CP-1 sample. Both C 1s and Fe 2p core levels of iron carbide species are marked with arrows. The presence of a shake-up peak at ca. 719 eV is the fingerprint of the Fe^{3+} species.

after NaOH addition. Mn^{2+} species coexisting along with these species will interact with these ferrihydrite-like solids, retarding hematite formation while forming poorly ordered solid solutions with the Fe oxide species that upon calcination develop Fe−Mn mixed oxides along with hematite phases. The maximum amount of Mn that can enter within the hematite lattice is about 15 mol %, and the rest of the Mn species will be deposited on the surface of the iron or iron−manganese oxide phases already formed, most likely as Mn^{4+} species.[21−27]

Magnetization curves are depicted in Figure 5. For the sake of comparison, magnetization values have been normalized to the mass of the sample. The magnetization curve of sample TG-70 resembles that of pure $MnFe_2O_4$, showing a superparamagnetic behavior at room temperature.[14] For this sample the magnetic moments of the nanoparticles change directions in unison with the direction of the applied magnetic field, showing a magnetization curve with near zero hysteresis and a very low coercitive field. From this magnetic behavior one can conclude that the sample consists mainly of $MnFe_2O_4$ units and no hematite-like domains. The low hysteresis (although still visible) of sample NP-70 together

(36) Stencel, J. M.; Diehl, J. R.; Miller, S. R.; Anderson, R. A.; Zarochak, M. F.; Pennline, H. W. *Appl. Catal.* **1987**, *33*, 129.

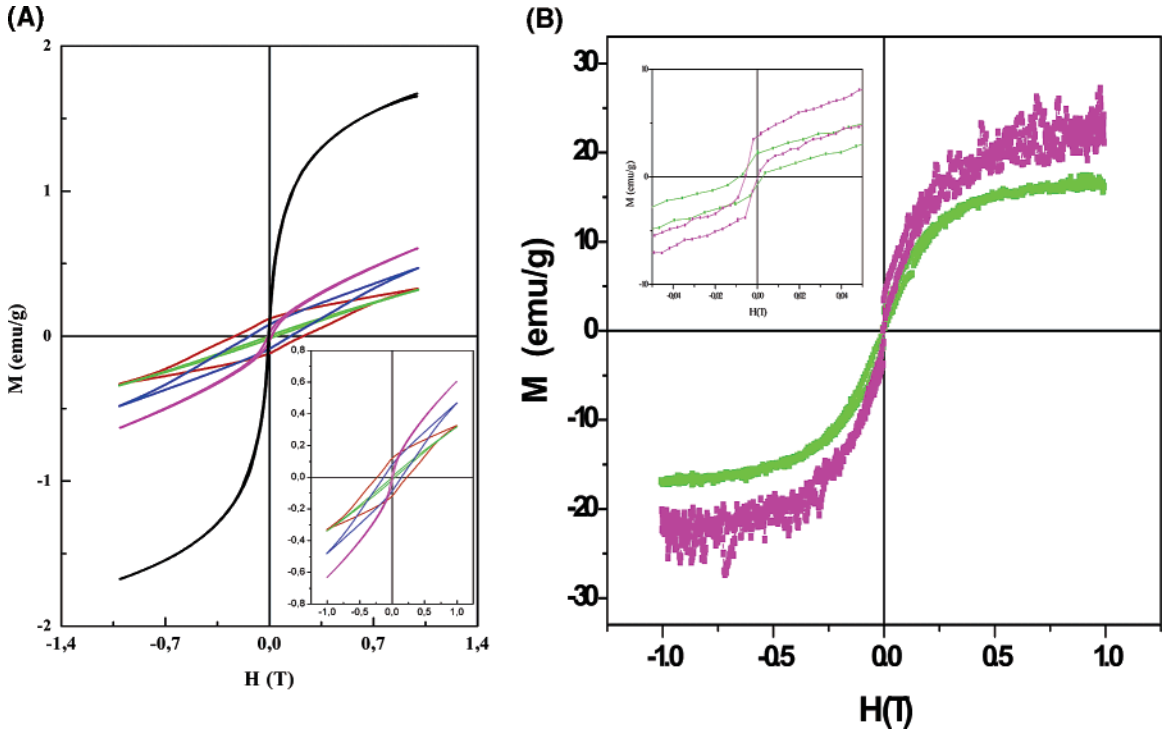

Figure 5. (A) Magnetization curves recorded at room temperature of selected samples. TG-70; NP-7; CP-1; PM-2; and 100Fe. (B) Magnetization curve of used samples (CP-1 and NP-70).

with its lower magnetization value in comparison with that of the previous sample could be attributed to a lower degree of Fe−Mn interaction and thus a lower superparamagnetic behavior (lack of a hysteresis loop). Most likely the sample would be a mixture of $MnFe_2O_4$ along with some Fe_3O_4 and Fe_2O_3 phases. It is well-known that replacing Fe by Mn in Fe_3O_4 usually increases the magnetization because the Mn ion has a higher magnetic moment.[37] Samples CP-1 and PM-2 display a magnetic behavior similar to that of α-Fe_2O_3 nanoparticles alone, showing a larger coercitive field, implying low Fe−Mn interaction. This reveals a predominant presence of hematite type particles unlike in the microemulsion series. Nonetheless, sample CP-1 shows a low coercitive value pointing toward the development of Fe−Mn interactions although its low magnetization value indicates that hematite-like but no magnetite-like species were obtained.

The magnetization behavior of used samples has been analyzed, namely, samples NP-70 and CP-1. Figure 5b depicts the magnetization of samples u-NP-70 and u-CP-1 (the prefix u- indicating that those are used samples). Clearly the magnetization of both used samples is larger than that of the "fresh" ones in agreement with the formation of Fe^0 species (most likely as iron carbide) during the reaction. Nevertheless, the magnetization behavior of used samples reveals a pattern the same as that of the fresh ones. That is, a higher magnetization value and a lower hysteresis cycle of the sample prepared by microemulsion, revealing that the homogeneity of the samples has not been drastically modified after the FT reaction. Nonetheless, it can be seen that the difference between the magnetization values of the used samples is not as large as it was for the fresh samples. This fact is due to a larger amount of reduced iron species present in sample u-CP-1 because, as discussed from the TPR results, the presence of Fe−Mn mixed oxides delayed the reduction process. This point somehow confirms the fact that Fe−Mn interaction is promoted for the samples prepared by the microemulsion methodology.

The particular nucleation behavior of the microemulsion based samples, in which precipitation is constrained within the water droplet, led to the formation of a large number of practically equal units of Mn surface enriched iron oxides. Although thermodynamically stable, within a microemulsion droplet the coalescence phenomenon is continuously taking place, and metal exchange is occurring yielding to a homogeneous distribution of metal (oxide) precursors within the medium. The solid obtained by the coprecipitation method (CP-1) under a non-pH-controlled environment displays a heterogeneous distribution of Fe and Mn phases. This feature is due local pH gradients affecting the nature of the hydrolyzed species formed.[38] In principle, if the pH is controlled during preparation it would be possible to obtain solids displaying a more homogeneous distribution of phases. Nevertheless, even if the pH was not controlled during the microemulsion route, relatively homogeneous solids were obtained. This accounts for the particular synthesis environment within the microemulsion. An even distribution of the metal precursors is stabilized within water droplets (provided microemulsions are formed). The addition of the precipitating agent triggers the formation of the oxide phases. This process modifies the pH of the environment affecting the nucleation of the vicinal species. However, because oxide formation is

(37) Wang, K. M.; Lee, D. S.; Horng, L.; Chern, G. *J. Magn. Magn. Mater.* **2004**, *282*, 73.

(38) Cornell, R. M.; Schwertmann, U. *The Iron Oxide*: *Structure, Properties, Reactions and Uses*; VCH Publishers: New York, 1996; Vol. 2, Chapter 13.

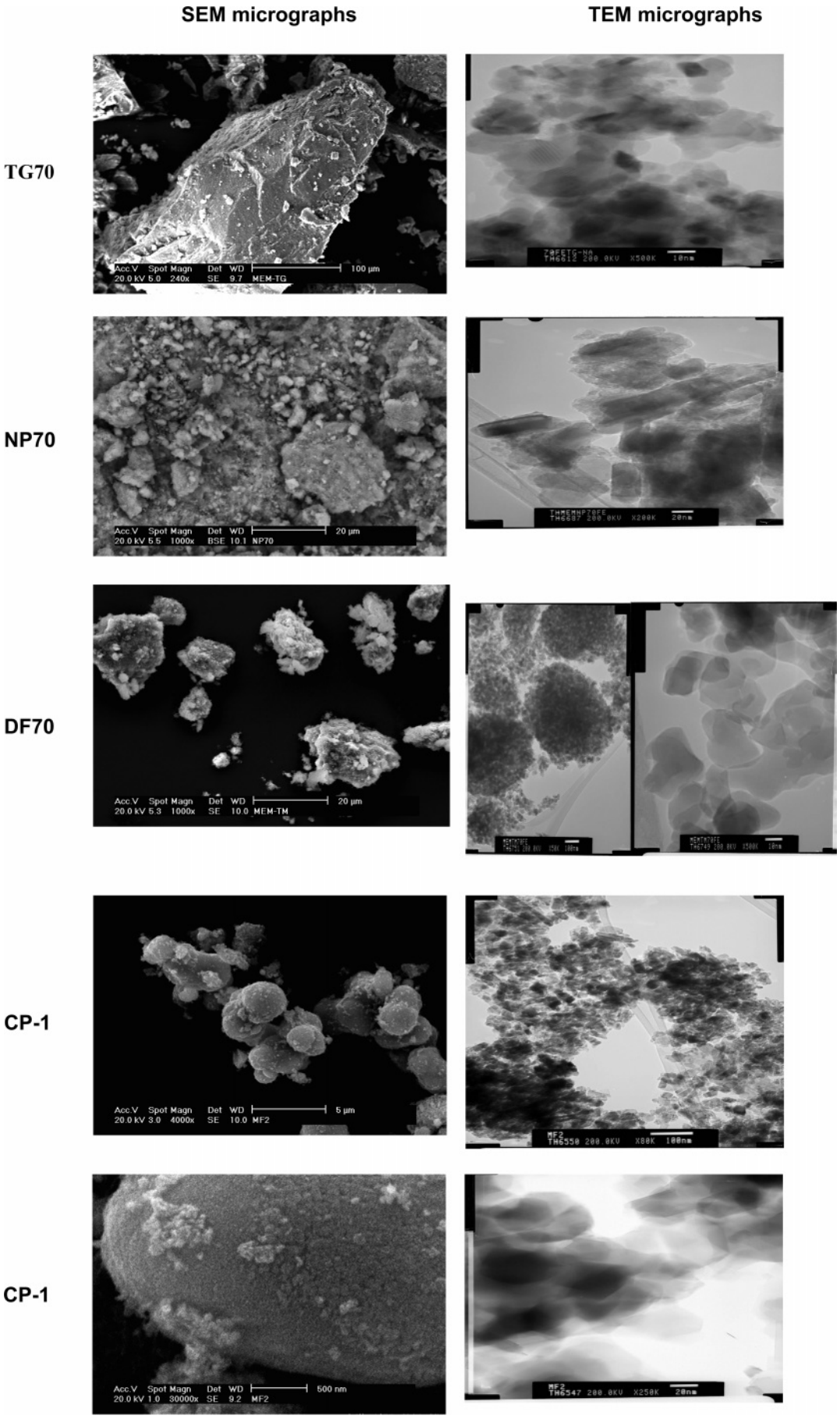

Figure 6. SEM and TEM pictures of selected samples.

Table 4. Catalytic Activity and Selectivity Compared at Similar Conversions[a]

						product selectivity (CO_2 free)			
catalyst	X_{CO} (%)	g_{CH_2}/g_{cat}·s	temp (K)	o/p	chain growth (α)	CH_4	C_2-C_5	gasoline (C_5-C_{12})	diesel (C_{13+})
100Fe	18.5	2.1×10^{-4}	518	1.2	0.56	6.0	68.5	31.5	0.1
PM-1	6.7	9.0×10^{-5}	518	2.5	0.54	5.8	66.3	28.7	0.4
CP-1	10.1	1.3×10^{-4}	573	5.5	0.47	7.3	69.7	23.1	0.4
PM-2	9.5	1.3×10^{-4}	518	1.7	0.57	6.7	66.2	30.7	0.7
TG-70	11.2	1.5×10^{-4}	573	5.4	0.59	6.6	65.9	25.7	1.1
NP-70	6.5	8.7×10^{-5}	573	2.0	0.58	7.2	64.5	28.9	0.9
NP-90	7.3	9.7×10^{-5}	573	1.8	0.58	7.4	65.7	31.6	1.1
KB-70	8.3	1.2×10^{-4}	573	2.6	0.59	7.1	58.8	31.5	2.6
DF-70	10.2	1.5×10^{-4}	573	2.5	0.57	7.5	61.2	30.8	2.5
X15-70	17.7	2.5×10^{-4}	573	3.0	0.57	6.7	61.2	31.5	3.0
AOT-70	1.5	2.1×10^{-5}	573	1.5	0.47	16.7	51.3	17.1	1.2

[a] X_{CO} = CO conversion; o/p stands for olefin-to-paraffin ratio; (α) chain growth probability.

constricted within isolated water droplets, concomitant pH modification will not affect vicinal water droplets that are actually separated by the presence of the surfactant and an oil phase. Thus, solids displaying homogeneous Fe−Mn oxide distribution from microemulsion can be obtained even if the pH is not controlled. Nonetheless, irrespective of the preparation route, not all Mn ions can enter within the Fe lattice. These features are consistent with the results obtained both from EDX and XPS analysis revealing (i) homogeneous distribution of Fe and Mn species, close to the stoichiometric value, and (ii) Mn surface enriched samples, respectively. It seems like a strong interaction between TG and the iron−manganese mixed oxide species is taking place, thus retarding hematite formation. An inhibitory effect of the organic matter on iron oxide crystallization has been reported already.[38,39] Results reported here, that is, iron oxide (either magnetite or hematite) formation impeded when prepared with TG, reveal that the interaction of the Fe oxyhydroxide species with such a surfactant is stronger than with any other of the series, remaining in the environment during the calcination step. Hematite like domains were detected by XRD and Raman analysis for samples prepared by physical mixture and coprecipitation and further confirmed by the magnetization experiments. These experiments also confirm that the degree of Mn substitution is larger in the TG-70 and NP-70 samples; actually, in the former a large amount of magnetite (either Mn substituted or not) was produced instead of hematite in accordance to the XRD, Raman, and TPR analysis. To a lesser extent, the nature of NP-70 is similar to that of TG-70; although Fe−Mn interaction has developed, the ratio of magnetite to hematite domains is lower.

On the other hand, metal distribution over the CP and PM series is heterogeneous; EDX analysis reveals Fe enriched zones coexisting along with Mn enriched ones. Figure 6 collects SEM and TEM micrographs of selected samples. Table 3 compiles the Fe and Mn contents from the EDX analysis. Again, Mn surface enrichment is detected by XPS and also observed from the TEM micrographs in which a thin layer covering of oxide particles is evident in most cases. The only exception to this pattern is sample PM-2 over which no Mn was detected by XPS analysis. In a similar manner, CP and PM sample preparation led to the formation of [$FeO(OH)_x$] species before Mn precipitation occurs, leading to Mn surface enriched samples.

Samples prepared by microemulsion consist of a large amount of round shaped particles, of about 10−20 nm closer to each other; meanwhile sample CP-1 consists of larger particles, the shape and distribution of the domains being more heterogeneous than those of the ones prepared by microemulsion and in a good agreement with our previous discussion concerning particle preparation route effect. Samples from the series PM displayed more edges than the microemulsion ones, which tend to be spherical although the nature of the surfactant also played a role. For instance, sample NP-70 displayed a rectangular shape.

To summarize the results obtained so far, microemulsion based samples are homogeneously distributed, most likely forming a mixed iron−manganese oxide solid with an intricate lattice over which Mn^{4+} species are deposited. Samples labeled as PM and CP are more heterogeneous; some solid solutions of different stoichiometry, along with a large amount of separate phases of iron oxide and manganese oxide, are detected. In either preparation the surface is enriched in Mn^{4+} species, although after H_2/CO treatment at 673 K, Mn enrichment diminishes, as revealed by XPS.

4. Catalytic Activity

The CO hydrogenation activity of selected samples has been tested in a fixed bed type reactor, and products were analyzed following manner similar to that described elsewhere.[40] Typically 0.11 g of sample is diluted in SiC (2.2 g) and pretreated at 553 K under 50 mL of syngas (H_2/CO = 2:1 molar ratio) for 1 h. The catalytic performance of the samples was monitored at 518 and 573 K at 1.0 MPa of H_2/CO (2:1 molar ratio) for 24 h. A summary of the catalytic results compared at similar conversions is collected in Table 4, while Figure 7 depicts the activity results obtained at 518 K. All catalysts were active in the FT synthesis yielding $-CH_2-$ units, along with CO_2, CH_4, and oxygenated products, irrespective of the reaction temperature studied. 100Fe and PM-2 were the most active samples, even despite the low surface area value of sample PM-2. When the reaction is carried at 573 K all samples displayed comparable performances toward $-CH_2-$ production; however, at lower temperatures the amount of FT product was larger over surface Mn free samples (namely, samples 100Fe and PM-2) probably due to the lack of activity of manganese

(39) Pizarro, C.; Escudey, M.; Fabris, J. D. *Hyperfine Interactions* **2003**, *148/149*, 53.
(40) Ojeda, M.; Granados, M. L.; Rojas, S.; Terreros, P.; Fierro, J. L. G. *J. Mol. Catal., A* **2003**, *202*, 179.

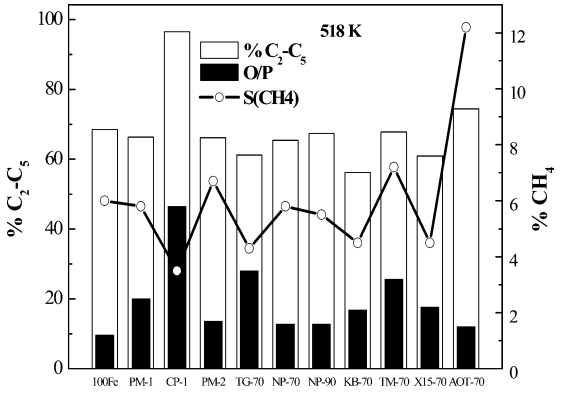

Figure 7. Methane conversion, selectivity to the C_2-C_5 fraction, olefin-to-paraffin ratio, and chain growth probability (α) for selected catalysts at 518 K.

oxide toward CO dissociation.[41] Hydrogenation ability, that is, methane production, was similar for all samples except for AOT-70; nonetheless, CO conversion over AOT-70 is too low to establish proper comparisons with the rest of the series.

The selectivity data confirm the tendency of Fe−Mn samples toward increasing the olefin-to-paraffin ratio (o/p)[41−43] of samples CP-1 and TG-70 displaying the highest values of about 5.5 of the series and among the largest values reported; for instance, the o/p value reported in the aforementioned study is 3.6 although at higher conversions. Similar results have been reported recently for a process conducted in the slurry phase.[44] The α factor (chain growth probability) and the C_5-C_{12} fraction production are also enhanced over samples prepared from microemulsion, especially when operating at 573 K. The α value for samples PM-1 and PM-2 at 573 K were 0.41 and 0.46, respectively, while it is higher than 0.6 for the microemulsion based samples at 518 K.

In terms of o/p value the results for sample CP-1 cannot be explained by Fe−Mn interaction alone. Even if in this sample such a mixed oxide phase is detected, the o/p value is comparable to that observed for sample TG-70 over which Fe−Mn interaction is maximized. This should bring into consideration the effect of the presence of Na onto the surface of these samples. As discussed in previous sections, Na was detected by XPS, its relative abundance with respect to Fe being about 0.15 and 0.22 for the microemulsion samples and CP-1, respectively. Thus, the high o/p ratio found for sample CP-1, with respect to the value found for the microemulsion based samples, is due to the presence of a higher amount of surface Na and its alkaline promotion.

It has been reported that alkaline promoters can modify the adsorption pattern of carbon monoxide on the active sites.[45] There have been recent attempts to study the effect of the different alkaline elements. The relative impact of the alkali metal depends on the conversion level potassium being the promoter that impacts the highest activity at all conversion levels. Na and K have the same effect at medium conversion (CO ca. 40%); the Na-promoted catalyst is less active than K-promoted ones at low conversions.[46] Therefore, K is the archetypical alkaline promoter and its effect has been extensively studied. It was concluded that K promotion consists of donating electronic density toward Fe sites. In this manner CO dissociation is favored and the Fe−CO bond is strengthened.[47] This CO dissociation enhancement is responsible for the modification of the selectivity of the obtained products such as an increment olefin-to-paraffin ratio and increase in high molecular product selectivity along the depletion of methane formation.[48]

As discussed above, Na is present in the surface of samples prepared with NaOH and it can be responsible of the high o/p value observed for CP-1 and samples prepared by microemulsion. For instance, the o/p values (measured as the $C^{=}_{2-4}/C_{2-4}$ fraction) reported by Yang et al.[47] for nonpromoted and for K (1.5 wt %)-promoted Fe/Mn (90:10 atom/atom) based catalyst are 1.5 and 7, respectively, confirming the tendency of alkaline promotion toward enhancing the o/p ratio. Such values cannot be straight compared to values reported in this paper due to the different activation and reaction conditions. Therefore, to establish proper comparison between different o/p and α values reported in this manuscript, samples CP-1 and TG-70 or NP-70 are compared. The α value found for sample CP-1 is lower than the ones observed for the microemulsion series (0.47 vs 0.59 or 0.58 for CP-1, TG-70, and NP-70, respectively), all of them being lower than those reported in the literature.[46,47] Therefore, it seems like the effect observed both in microemulsion prepared samples and in CP-1, that is, the increase in both olefin and C_5-C_{12} production, is due to the Mn rather than to the presence of residual sodium alone. Actually, due to its alkaline character, Mn can promote CO dissociation, enhancing the amount of $-CH_2-$ type species and at the same time decreasing the amount of adsorbed hydrogen species, thus lowering the hydrogenation ability of the samples, enhancing the o/p ratio and favoring chain growth, while at the same time inhibiting secondary reactions such as isomerization and hydrogenation. Nonetheless, if Mn addition improves Fe dispersion (the active component) suppressing carbon chain growth,[49] the overall performance of the catalysts would be a balance of both effects, and this last effect could be the most important.

5. Conclusions

Preparation of mixed iron−manganese oxide by the microemulsion technology renders more homogeneous samples consisting of small-sized round particles than traditional routes; furthermore, Fe−Mn interaction is enhanced when samples are prepared by this technology. Surfaces are enriched in Mn, most likely as Mn^{4+} species although after H_2/CO treatment the amount of surface iron species is

(41) Jensen, K. B.; Massoth, F. E. *J. Catal.* **1985**, *92*, 98.
(42) Malessa, R.; Baerns, M. *Ind. Eng. Chem. Res.* **1988**, *27*, 279.
(43) Ji, Y.-Y.; Xiang, H.-W.; Yang, J.-L.; Xu, Y.-Y.; Li, Y.-W; Zhong, B. *Appl. Catal., A* **2001**, *214*, 77.
(44) Bai, L.; Xiang, H.-W.; Li, Y.-W.; Han, Y.-Z.; Zhong, B. *Fuel* **2002**, *81*, 1577.
(45) Williams, F. R.; Lambert, R. M. *Catal. Lett.* **2003**, *70*, 9.
(46) Ngantsoue-Hoc, W.; Zhang, Y. Q.; O'Brien, R. J.; Luo, M. S.; Davis, B. H. *Appl. Catal., A* **2002**, *236*, 77.
(47) Yang, Y.; Xiang, H. W.; Xu, Y. Y.; Bai, L.; Li, Y. W. *Appl. Catal., A* **2004**, *266*, 181.
(48) Anderson, R. B. In *Catalysis IV*; Emmet, P. H., Ed.; 1956; pp 2−19.
(49) Kölbel, H.; Ralek, M. *Catal. Rev.—Sci. Eng.* **1980**, *21*, 225.

enhanced. The samples are active in the FT synthesis producing mainly hydrocarbons, promoting the production of the gasoline fraction and enhancing the olefin-to-paraffin ratio. The catalytic performance of the samples depended on the Fe/Mn atomic ratio and partially in its location within the sample. Nevertheless, to promote Fe effect in the FT synthesis only relative extension of the Fe−Mn interaction will suffice.

Acknowledgment. S.R. acknowledges the Programa Ramón y Cajal from the Spanish Ministerio de Ciencia y Tecnología for financial support. F.J.P.-A. also thanks the Spanish Ministerio de Ciencia y Tecnología for financial support. Financial support under Project No. ENE-2004-07345-C03-01/ALT is also acknowledged.

CM052568I